Degradation of polystyrene plastics by alkane monooxygenase and alcohol dehydrogenase

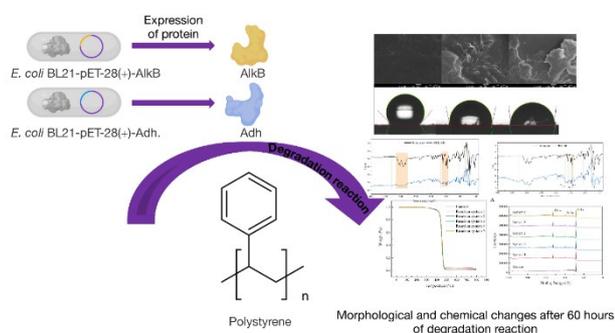**Yue Gao[a], Beixi Liu[a], Yan Deng[a], Anhong Yu[a], Huimin Ye[a], Ying Zhang[a] and Liang Kong[a]***

[a]College of Marine Technology and Environment, Dalian Ocean University, 52 Heishijiao Street, Dalian 116023, Liaoning, China.

*to whom all correspondence should be addressed: e-mail: 897207100@qq.com

Graphical abstract

Abstract

The consumption of plastic products has led to the generation of large amounts of plastic waste, which is persistent and difficult to degrade. Polystyrene (PS) is one of the six most important plastics in the world and is difficult to degrade in the environment owing to its high stability. To investigate PS degradation by biological enzymes, two oxidoreductases, alkane hydroxylase (AlkB) and alcohol dehydrogenase (Adh), were selected from the bacterial strain *Acinetobacter johnsonii* JUN01, which has been proven to be capable of degrading PS. Genetically engineered bacteria capable of expressing AlkB and Adh were constructed using genetic engineering technology, and the degradation activities of AlkB monoenzyme, Adh monoenzyme, and AlkB–Adh composite enzyme were investigated. Thermal field emission scanning electron microscopy (SEM) and water contact angle (WCA) measurements demonstrated that the investigated enzymes transformed PS from hydrophobic to hydrophilic. Fourier transform infrared (FTIR) results showed that after enzymatic hydrolysis, the number of hydroxyl groups (–OH) increased, the number of C=C and C=O bonds increased, and the structure of benzene ring was disrupted by degradation using AlkB monoenzyme and AlkB–Adh composite enzyme. X-ray photoelectron spectroscopy (XPS) showed that the characteristic C–C bonds of PS decreased, and the number of C–O bonds and C=O bonds increased. The molecular weight of PS changed after digestion, as determined by high-temperature gel chromatography (GPC). Thermogravimetric analysis (TGA) was used to demonstrate a decrease in the thermal stability of PS after digestion. These results showed that the AlkB monoenzyme, Adh monoenzyme, and AlkB–Adh composite enzyme all had PS degradation activity, demonstrating that the idea of using a composite enzyme to degrade PS was feasible. In addition, Adh exhibited degradation activity in two different coenzyme reaction systems. Therefore, these results provide a theoretical basis and data support for the future degradation of PS by bioenzymes.

Keywords: Plastic degrading enzymes; Microplastics; Biodegradation

1. Introduction[1]

Hazards triggered by the extensive use of plastics have gained global attention, with more than 350 million tons of plastics produced globally in 2019 (Orona-Návar *et al.* 2022). In addition, the use of single-use plastics has been exacerbated by this new COVID-19 epidemic. In March 2020, 3.4 billion disposable masks were discarded globally daily, and the demand for plastic products, such as disposable gloves, bottled water, disposable wipes, hand sanitizer, and detergents, was unprecedented, generating 1.6 million tons of plastic waste globally daily (Benson *et al.* 2021). The consumption of plastic products generates large amounts of plastic waste. Plastics are difficult to degrade and persist in nature. During their long-term existence in nature, plastics gradually undergo weathering forming plastic fragments, and these microplastics are more

---

[1] polyethylene glycol terephthalate (PET), polyethylene (PE), polystyrene (PS), polypropylene (PP), alkane hydroxylase (AlkB), alcohol dehydrogenase (Adh), scanning electron microscopy (SEM), water contact angle (WCA), Fourier transform infrared (FTIR), X-ray photoelectron spectroscopy (XPS), high-temperature gel chromatography (GPC), thermogravimetric analysis (TGA), tetrahydrofuran (THF), number-average molecular weight (Mn), heavy-average molecular weight (Mw), theoretical isoelectric point (pI)

---

harmful to the ecological environment than the normal-sized plastics. Microplastics refer to plastic particles and fragments with diameters less than 5 mm (Gabisa and Gheewala 2022). In addition to the aforementioned microplastics formed by natural weathering, they are also generated by human production of cosmetics and clothing and found in both industrial and municipal wastewater. Studies have shown that fibers and fragments are the main types of microplastics, with PET, PE, PS, and PP being the most common (Gabisa and Gheewala 2022). Microplastics are small, widespread and abundant, and ability to adsorb toxic substances, making them more hazardous than normal-sized plastics (Verla *et al.* 2019). Microplastics seriously jeopardize the environment and human health. PS is a man-made aromatic polymer polymerized from styrene monomers (Zhang *et al.* 2021) with the molecular formula $(C_8H_8)_n$. In addition, PS is one of the top six most important plastics in the world and has good corrosion resistance and high stability. Owing to its good mechanical properties and relatively low cost, PS is widely used in construction materials, packaging foam, and disposable tableware. However, PS is not easily degraded in the environment because of its high stability. Therefore, PS degradation is a critical global issue.

Traditional plastic disposal methods include landfilling, incineration, and recycling (Peng *et al.* 2018). The disadvantages of the landfill method are that plastics that are difficult to degrade, take up land resources, and produce toxic and hazardous substances that pollute the soil and groundwater. The advantage of incineration is that energy is recovered by burning waste, which can completely or partially offset the energy consumed in the heating process. However, the recycling value is low, and toxic gases such as carbon monoxide, nitrogen oxides, and soot are produced, which cause secondary pollution. A disadvantage of this recycling method is that there are many different types of plastics, and categorizing them for recycling is difficult. However, chemical recycling has the disadvantage of high energy consumption. Therefore, traditional physical and chemical recycling methods, which are used for the treatment of large plastics, have drawbacks. In addition, the above recycling methods will produce microplastics during the recycling process, which are even more harmful than large plastics.

Currently, biodegradation is the most effective, innovative, and eco-friendly method for degrading microplastics. Biodegradation usually refers to removing microplastics from the environment by using microorganisms or their active products (enzymes). In addition, biodegradation is a plastic waste treatment method that can be carried out in-situ, is green, and has a relatively low-cost. The main mechanism of biodegradation is oxidative degradation, which reduces the molecular weight of plastic materials, usually after the enzymatic decomposition of organic substances, catalyzing the cleavage of polymer bonds into monomers, thus achieving the purpose of degrading plastics (Chaurasia 2020).

At the present time, it is reported that the biodegradation of PS is mainly carried out by bacteria. As early as 1999, Kiatkamjornwong *et al.* found that *Bacillus coagulans* was able to degrade composite PS sheets made from graft copolymers of tapioca starch and PS (Kiatkamjornwong *et al.* 1999). *Serratia marcescens*, *Pseudomonas sp.*, *Bacillus sp.*, *Staphylococcus aureus*, *Streptococcus pyogenes*, *Klebsiella sp.* and *Citrobacter sp.* can degrade PS (Galgali *et al.* 2002; Oikawa *et al.* 2003; Atiq *et al.* 2010; Asmita *et al.* 2015; Mohan *et al.* 2016; Subramani and Sepperumal, 2017; Yang *et al.* 2020; Urbanek *et al.* 2020; Kim *et al.* 2020a). Compared with PS-degrading bacteria, studies on PS-degrading fungi have been less reported in recent years and appeared at a later time. The main fungi that have been identified and are capable of degrading PS are *Aspergillus niger* and *Cephalosporium* (Kong *et al.* 2018; Chaudhary *et al.* 2020). Meanwhile, few reports on PS-degrading enzymes exist. Research reports on biological enzymes for PS degradation have mainly focused on the theoretical speculative level, and few target enzymes are expressed by genetic engineering techniques, and enzyme activity is explored. Furthermore, the degradation mechanism is still unclear. Most microplastic-degrading enzymes function through the depolymerization of long carbon chains of plastic polymers into mixtures of oligomers, dimers, and monomers (Amobonye *et al.* 2021). Hydrolases and oxidoreductases are important plastic-degrading enzymes. Alkane hydroxylases, monooxygenases, cytochrome P450, aromatic ring hydroxylases, laccases, esterases, and α/β hydrolases are the main enzymes widely present in microorganisms capable of degrading PS, but esterases and α/β hydrolases may not play a large role in the degradation of PS due to the absence of ester bonds (Hou and Majumder, 2021; Anastasia, 2023).

Most microplastic-degrading enzymes come from bacteria or fungi. In bacteria or fungi, multiple enzymes usually work together to degrade microplastics. Some degradative enzymes are involved in heterogeneous reactions occurring at the solid–liquid interface, acting on macromolecules on the surface of solid plastics, whereas others are responsible for the degradation of metabolic intermediates of plastics into unit monomers or for the final mineralization of plastics (Amobonye *et al.* 2021). There are few reports on the degradation of microplastics by complex enzymes, and these studies are preliminary explorations. Studies on the complex enzymatic degradation of microplastics have mainly focused on PET, the most cutting-edge of which is the identification of two enzymes capable of hydrolyzing PET (Yoshida *et al.* 2016) in the bacterium *Ideonella sakaiensis* 201-F6, which efficiently converted PET into two environmentally benign monomers, terephthalic acid and ethylene glycol. During the degradation process, PETase first breaks down PET into mono(2-hydroxyethyl) terephthalate, which is further broken down into the monomers terephthalic acid and ethylene glycol by MHETase. The two enzymes were then expressed with recombinant *E. coli* to compare the degradation of PET by mono- and composite enzymes, demonstrating that monoenzymes were less effective than composite enzymes in degrading PET, which provided research insights for this study. As negligible reports on composite enzyme degradation studies of PS exist, to fill

the gap regarding the synergistic degradation of PS by biological enzymes, we explored the degradation activities of AlkB and Adh on PS. Theoretically, AlkB is responsible for catalyzing the hydroxylation of PS, which is considered to be the first step in the degradation of PS (Liu *et al.* 2014), and Adh acts on the hydroxyl group to cause it to form other chemical bonds; therefore, a combination of the two enzymes may achieve better results for the degradation of PS.

In this study, the key enzymes predicted to be responsible for the degradation of PS, alkB (Protein_id AZN63878.1) and adh（Protein_id AZN64220.1）, were synthesized using genetic engineering techniques from the bacterial strain *Acinetobacter johnsonii* JNU01, which has been shown to degrade PS (Kim *et al.* 2021). To investigate the changes in the physicochemical properties of PS before and after the degradation of AlkB, Adh, and AlkB–Adh, the present study was carried out using thermal field emission scanning electron microscopy (SEM), water contact angle (WCA) analysis, Fourier transform infrared (FTIR), X-ray photoelectron spectroscopy (XPS), high-temperature gel chromatography (GPC), and thermogravimetric analysis (TGA). This study aims to provide ideas and directions for future research on PS-biodegrading enzymes to safely and effectively address the pollution and hazards caused by PS in the environment.

2. Materials and methods

2.1. Bacterial strain and plasmid

The bacterial strain used in this study was *E. coli* BL21 (DE3), the target genes were alkB (Protein_id AZN63878.1) and adh (Protein_id AZN64220.1) from *A. johnsonii* JUN01 (GenBank accession number CP022298.1), and the expression vector was pET-28a(+) (AZN64220.1), which was synthesized by codon optimization according to the characteristics of *E. coli*. The bacterial strain, target gene AlkB, and vector were obtained from the Sangong Bioengineering (Shanghai) Co. Ltd, and the target gene Adh was synthesized by the Jiu Tian Gene Technology Co. (Tianjin, China). The synthesis was optimised according to the characteristics of *E. coli*.

2.2. Synthesis, induced expression, and enzyme solution preparation of recombinant E. coli

The pET-28a(+)-AlkB plasmid was transfected into *E. coli* BL21 (DE3) receptor cells to obtain recombinant *E. coli* BL21-pET-28a(+)-AlkB. The strains were stored in glycerol at a final concentration of 25% in a -80℃ refrigerator. The recombinant *E. coli* was inoculated into TB medium containing a final concentration of 50 mg/L kanamycin and cultured overnight at 37°C and 180 rpm; the seed medium was inoculated into TB medium containing a final concentration of 50 mg/L kanamycin with an inoculum volume of 2% and cultured at 37°C and 180 rpm. When the OD_{600} of the bacterial solution was 0.6~0.8, the isopropyl β-D-1-thiogalactopyranoside inducer was added at a final concentration of 1 mM, and the expression was induced for 20 h at 18℃ and 180 rpm. The bacteria was collected by centrifugation (5000 rpm, 15 min, 4℃), the collected bacteria was resuspended in 50 mM Tris-HCl (pH of 7.0), and the cell was broken by using an ultrasonic crusher (ice bath) to the point that the bacterial solution was transparent, followed by additional centrifugation (7000 rpm, 20 min, 4°C) to obtain the supernatant (i.e., crude enzyme solution).

2.3. Microplastics

PS with a particle size of 48 μm was purchased from the Dongguan Zhangmutou Ruixiang Polymer Material Co. The PS was washed with 10% aqueous methanol solution, dried completely in a constant temperature blast drying oven at 60℃, and sterilized by the ultraviolet light sterilization method for spare parts.

2.4. Degradation reaction system

The reaction conditions were 37°C, 200 rpm, and 60 h. The control only contained PS, coenzymes, and Tris-HCl buffer in the reaction solution but did not contain any biological enzymes. Reaction system 1 was AlkB monoenzyme degradation, and the reaction solution consisted of 50% (v/v) AlkB crude enzyme solution (453 μg/mL), 0.1 g of PS, 50 mM Tris-HCl (pH of 7.5), 1 mM MgSO4, 1 mM NADH, and 0.1 mM FAD. The effects of two coenzymes, NAD and NADH, on the Adh degradation of PS were investigated since the reaction mechanism of Adh degradation of PS is still unknown. Reaction systems 2 and 3 were used to degrade the Adh monoenzyme. The reaction solution for reaction system 2 consisted of 50% (v/v) Adh crude enzyme solution (432 μg/mL), 0.1 g of PS, 50 mM Tris-HCl (pH of 7.5), and 1 mM NAD. Reaction system 3 consisted of 50% (v/v) Adh crude enzyme solution (432 μg/mL), 0.1 g of PS, 50 mM Tris-HCl (pH of 7.5), and 1 mM NADH. Reaction systems 4 and 5 used the AlkB–Adh complex enzymatic solution. The reaction solution of reaction system 4 included 25% (v/v) AlkB crude enzyme solution (453 μg/mL), 25% (v/v) Adh crude enzyme solution (432 μg/mL), 0.1 g of PS, 50 mM Tris-HCl (pH of 7.5), 1 mM NAD, 1 mM NADH, 0.1 mM FAD, and 1 mM MgSO$_4$. The reaction solution of reaction system 5 included 25% (v/v) AlkB crude enzyme solution (453 μg/mL), 25% (v/v) Adh crude enzyme solution (432 μg/mL), 0.1 g of PS, 50 mM Tris-HCl (pH of 7.5), 2 mM NADH, 0.1 mM FAD, and 1 mM MgSO₄.

2.5. Washing and drying of samples

The reacted PS was washed three times with an aqueous solution containing 10% methanol and 2% SDS solution, and the washed PS was completely dried in a constant temperature blast drying oven at 60°C.

2.6. Analysis procedure

2.6.1. Western blotting

Target protein expression was verified by western blotting (BIO-RAD Mini-PROTEAN Tetra 552BR145889, USA). The recombinant His-Tag was bound to a His monoclonal antibody, then to a secondary antibody, and finally imaged using a gel system imager (Tanon-2500R, China) to verify the successful expression of the target protein.

2.6.2. SEM

Scanning electron microscopy (SEM, JEOL JSM-7610F-Plus, Japan) was used to observe the changes in the surface

morphology of the PS particles before and after the enzymatic reaction. The samples were subjected to conductive treatment, i.e., a metal film was sprayed on the surface of the samples to make the samples electrically conductive; and finally SEM was performed to observe the samples.

2.6.3. FTIR

The changes in the molecular structure of PS before and after enzymatic digestion were analyzed using FTIR (Agilent Cary 600 Series, USA). The samples and potassium bromide were fully ground under infrared lamps and then placed into a mold, which was placed onto a tablet press. The diaphragm vacuum pump was turned on to perform the pressing, and the scans were carried out after the completion of the pressing.

2.6.4. XPS

C and O elemental analysis of PS using XPS (Thermo EscaLab 250Xi, USA). The cleaned and dried PS samples were pasted on conductive adhesive tape and then placed on the sample stage. After the samples entered the instrument compartment, they were placed under a vacuum prior to the analysis. The tested elements were C, N, and O. The XPS tests were performed using a Thermo EscaLab 250Xi instrument (USA).

2.6.5. WCA measurement

The WCA (Kino SL250, USA) of the PS was measured before and after the enzymatic reaction to observe the degree of change. Ultrapure water was used to test the PS. The samples were pressed and processed on a horizontal table, water droplets to be tested were added, and images of the water droplets were captured with a video camera, followed by importation into the software for analysis.

2.6.6. GPC

The molecular weight changes in PS before and after the enzymatic reaction were analyzed using GPC (Waters 2414, USA). PS before and after the enzymatic reaction was solubilized with THF and filtered through a 0.2 µm ultrafiltration membrane. The test conditions were: mobile phase, THF; flow rate, 1 mL/min; temperature, 30°C; and injection volume, 30 µL.

2.6.7. TGA

The change in the thermal stability of PS before and after the enzymatic reaction was analyzed by TGA (TGA Q50, USA). The test conditions were: temperature range from 30°C to 800°C; ramp rate, 10°C/min; and gas atmosphere, nitrogen.

3. Results and discussion

3.1. Protein expression verification

The alkB gene consists of 1197 bp, encodes the AlkB enzyme of 398 amino acids, with a pI of 9.4, and a predicted molecular weight of 45 kDa. And the adh gene consists of 1161 bp, encodes the Adh enzyme of 386 amino acids, with a pI of 5.8, and a predicted molecular weight of 42.1 kDa. Successful expression of AlkB and Adh was demonstrated by Western blotting and their molecular weight were analysed as shown in **Figure 1**. Compared with the

organisms not containing the vectors pET-28a(+)-AlkB and pET-28a(+)-Adh, *E. coli* BL21-pET-28a(+)-AlkB and *E. coli* BL21-pET-28a(+)-Adh showed distinct bands at 45 and 42.1 kDa, respectively, which were consistent with the expected protein molecular weights size was basically consistent, indicating successful protein expression.
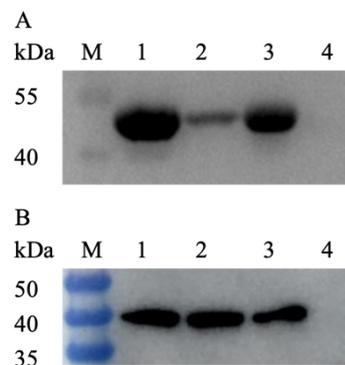
Figure 1. Western blotting results of *E. coli* BL21-pET-28a(+)-AlkB (A) and *E. coli* BL21-pET-28a(+)-Adh (B). (Lane M: marker, Lanes 1–4: whole cells containing the gene of interest, supernatant containing the gene of interest, broken precipitate containing the gene of interest, and whole cells without load)

3.2. SEM analysis of PS

The surface morphology of PS after treatment with different reaction systems is shown in **Figure 2**. The surface of the PS in the blank control group was relatively smooth with no obvious cracks or grooves. After the enzymatic reaction, the surface of the PS particles became much rougher, with grooves, erosion, and fragmentation. All of these phenomena indicated that AlkB, Adh, and AlkB–Adh had degradation effects on PS and that both Adh and AlkB–Adh could exert their catalytic effects under different coenzyme conditions.
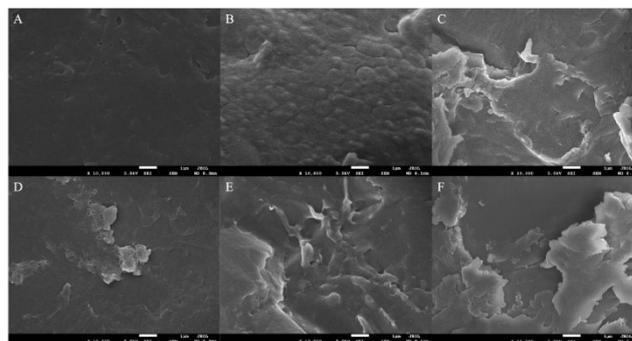
Figure 2. SEM images of PS after 60 h of biodegradation. (A: Control, B: Reaction system 1, C: Reaction system 2, D: Reaction system 3, E: Reaction system 4, F: Reaction system 5).

3.3. WCA analysis of PS

To determine the effect of different reaction systems on the hydrophobicity of PS, PS was measured before and after the enzymatic reaction using a WCA instrument. As shown in **Figure 3**, the WCA of the blank control group was 131.040°, indicating significant hydrophobicity owing to its linear carbon skeleton. The WCAs of PS after enzymatic degradation were smaller than that of the blank control group. The PS WCAs after degradation were 103.973°,

101.692°, 101.188°, 101.830°, and 94.769° for reaction systems 1–5, respectively. The smaller the WCA, the more hydrophilic the surface of the material, which indicates that the degradation of PS by the AlkB monoenzyme, Adh monoenzyme of different reaction systems, and AlkB–Adh composite enzyme all resulted in a shift of PS from hydrophobic to hydrophilic. An increase in surface hydrophilicity is essential for microorganisms and their active products to attach to the PS surface and form biofilms (Arunrattiyakorn *et al.* 2022; Cheng *et al.* 2022), further demonstrating the degradation activity of AlkB, Adh, and AlkB–Adh complex enzymes on PS. Therefore, the WCA measurements verified that enzymatic digestion enhanced the hydrophilicity of the PS surface.

Figure 3. WCA analysis of PS after 60 h of biodegradation. (A: Control, B: Reaction system 1, C: Reaction system 2, D: Reaction system 3, E: Reaction system 4, F: Reaction system 5).

3.4. FTIR analysis of PS

To further understand the effects of AlkB, Adh, and AlkB–Adh composite enzymes on the molecular structure of PS, the PS from the blank control group and the experimental groups were analyzed using FTIR.

The absorption peaks of PS in the blank control group at 3100–3000 cm^{-1} are the telescopic vibration of benzene ring C–H, while the absorption peaks at 3000–2800 cm^{-1} are the telescopic vibration of saturated alkyl C–H. Meanwhile, the absorption peaks at 2350 cm^{-1} is attributed to the antisymmetric stretching vibration of CO_2 adsorbed in air, and the absorption peaks at 2000–1700 cm^{-1} is correlated with the octave frequency of the deformation vibration of the benzene ring C–H. The absorption peaks at 1592 and 1488 cm^{-1} are benzene ring skeleton vibrations; the absorption peaks at 1445, 1370, and 1313 cm^{-1} are attributed to C–H bending vibrations; the absorption peaks between 1250 and 800 cm^{-1} are corresponds to C–C stretching vibrations and benzene ring C–H in-plane bending vibrations; and the absorption peaks at 750 and 690 cm^{-1} are benzene ring monosubstituted C–H out-of-plane bending vibrations.

AlkB is a typical alkane hydroxylase that contributes to the first step of PS mineralization, acting mainly on the β-carbon of the carbon chain and playing a major role in main chain cleavage (Kim *et al.* 2021). As shown in **Figure 4(A)**, PS particles degraded by AlkB for 60 h exhibited a broad absorption peak at 3300 cm^{-1} corresponding to the O–H stretching vibration. The absorption peak at 1666 cm^{-1} corresponded to the C=C or C=O stretching vibration. The absorption peaks corresponding to the benzene ring backbone vibration were weakened at 1592 and 1488 cm^{-1}, and the absorption peak corresponding to the C–H bending vibration was weakened at 1445 cm^{-1}. This indicates that some of the benzene ring structure was destroyed and a C=C double bond or C=O double bond was generated. The absorption peak at 1070 cm^{-1} increased, which might be caused by the stretching vibration of the C–

O bond. These changes confirmed the degradation activity of AlkB on PS.

The FTIR spectra of the PS degraded by Adh for 60 h are shown in **Figure 4(B) and (C)**. The results of the FTIR plots of reaction system 2 revealed that the curve changes were not significant when using Adh to degrade PS, and changes only occurred at approximately 3300 and 1660 cm^{-1}; the broad absorption peak at 3300 cm^{-1} corresponds to the O–H stretching vibration, and the absorption peak at 1666 cm^{-1} corresponds to the C=C or C=O stretching vibration.

Reaction system 3 shows that the curve change is insignificant and is similar to that of reaction system 2. Significant changes were only observed near 3300 and 1660 cm^{-1}, with the broad absorption peak at 3300 cm^{-1} corresponding to the O–H stretching vibration and the absorption peak at 1666 cm^{-1} attributed to the C=C or C=O stretching vibration. These changes indicate that the degradation of PS using Adh alone was equally active in both reaction systems, but the molecular structure of the enzymatically degraded PS changed little.

The changes in the molecular structure of PS in composite enzymatic reaction system 4 are shown in **Figure 4(D)**, with a weak broad absorption peak at 3300 cm^{-1} corresponding to the O–H stretching vibration. The absorption peaks corresponding to unsaturated C–H bonds at 3100~3000 cm^{-1} become weaker but more numerous, and the change in this position is likely due to the generation of olefins, which are the result of the olefin=CH stretching vibration. The absorption peaks at 3000~2800 cm^{-1} change, which is attributed to the saturated C–H stretching vibration. The change in the absorption peak at 3000~2800 cm^{-1} was due to the change in the saturated alkyl C–H bonds. The absorption peak at 1666 cm^{-1} corresponds to a C=C or C=O stretching vibration. The absorption peak at 1070 cm^{-1} increases, which may be due to the stretching vibration of the C–O bond. The absorption peak at 838 cm^{-1} is significantly enhanced, which may be caused by the out-of-plane bending vibration of the olefin C–H, combined with the change in the shape of the monosubstituted peaks of the benzene ring at 750 and 690 cm^{-1}. The peak at 838 cm^{-1} becomes stronger, possibly due to a change in the substitution mode of part of the benzene ring.

The changes in the PS molecular structure of reaction system 5 are shown in **Figure 4(E)**, with a broad absorption peak at 3300 cm^{-1} corresponding to the hydroxyl O–H stretching vibration, an absorption peak at 1666 cm^{-1} corresponding to the C=C or C=O stretching vibration, weakened absorption peaks corresponding to the benzene ring backbone vibration at 1592 and 1488 cm^{-1}, and a weakened absorption peak corresponding to the C–H bending vibration at 1445 cm^{-1}, indicating that some of the benzene ring structure was destroyed and a C=C or C=O double bond was generated. Additionally, the absorption peak at 1070 cm^{-1} increased, which might be caused by the stretching vibration of the C–O bond. This indicates that AlkB–Adh has PS degradation activity, but the changes in the molecular structure of PS vary in the different coenzyme systems.
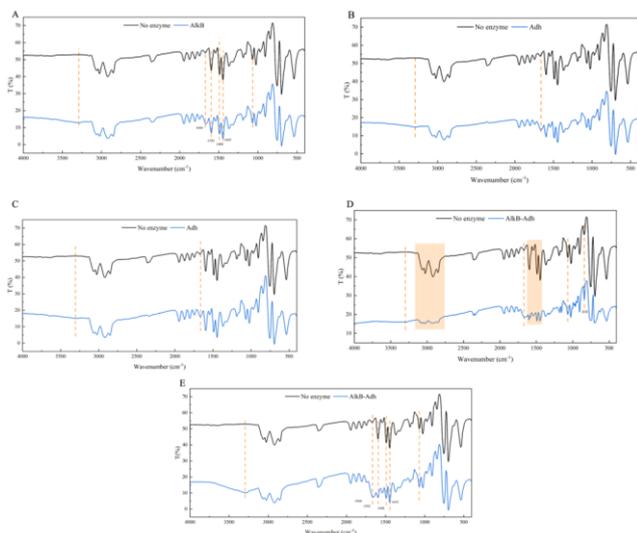
Figure 4. FTIR image of PS after 60 h of biodegradation. (A: Reaction system 1, B: Reaction system 2, C: Reaction system 3, D: Reaction system 4, E: Reaction system 5).

3.5. 3.5 XPS analysis of PS

XPS was used to analyze changes in the chemical composition and functional groups on the surface of the PS particles before and after enzymatic digestion. **Figure 5(A)** shows the XPS scanning broad spectra of PS from the blank control group and five reaction systems. The spectrum of the blank control group only had an elemental carbon peak at 284 eV, while the spectra of enzymatically digested PS had distinct peaks at 531 eV attributed to elemental oxygen.

The XPS C1s spectra of PS from the blank control group and five reaction systems were subsequently analyzed, as shown in **Figure 5(B)**. These spectra mainly show the presence of surface carbon with elemental carbon-related functional groups. The C–C bond peak (284.8 eV) was significantly reduced after the enzymatic reaction, with the most obvious reduction of the C–C bonds on the surface of PS after AlkB–Adh composite enzyme degradation in reaction system 5, while relatively little change in the C–C bonds was observed after degradation by the Adh single enzyme. This is consistent with previous reports; that is, AlkB is responsible for the first step of PS mineralization, which involves disrupting the carbon chain of PS and hydroxylating PS, whereas Adh catalyzes the conversion of hydroxyl groups to other chemical bonds. Therefore, AlkB is mainly responsible for the destruction of the C–C bonds, and the destruction of the C–C bonds is the most significant when the two enzymes degrade synergistically.

Compared to the blank control group, the C=O (288.2 eV) and C–O (286.6 eV) bonds on the surface of PS increased after enzymatic degradation, with the most significant increase during the synergistic enzymatic degradation of reaction system 5. The generation of C–O bonds after enzymatic hydrolysis implies that some of the C–C bonds in PS were oxidized to alcohols and carboxylic acid-like compounds (Shang *et al.* 2003). These analyses indicate that some of the C–C bonds are replaced by C=O and C–O bonds during enzymatic hydrolysis. The formation of C=O bonds or other similar oxygen-containing functional groups

is the main indicator of PS degradation. This suggests that AlkB, Adh and AlkB-Adh can all oxidise PS to form derivatives and change the surface properties of PS from hydrophobic to hydrophilic (Kim *et al.* 2020b).
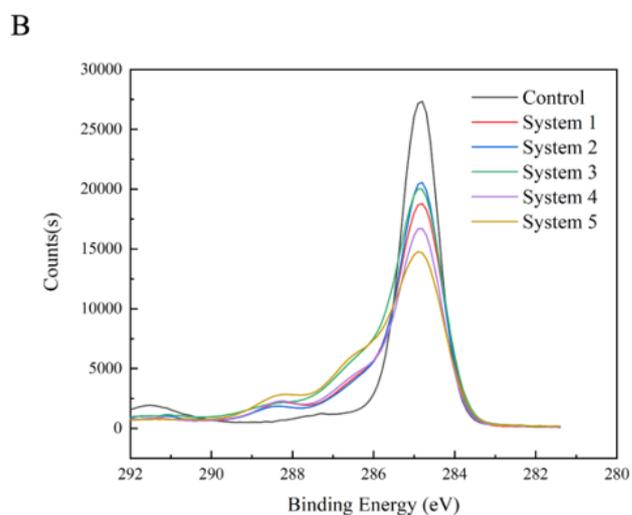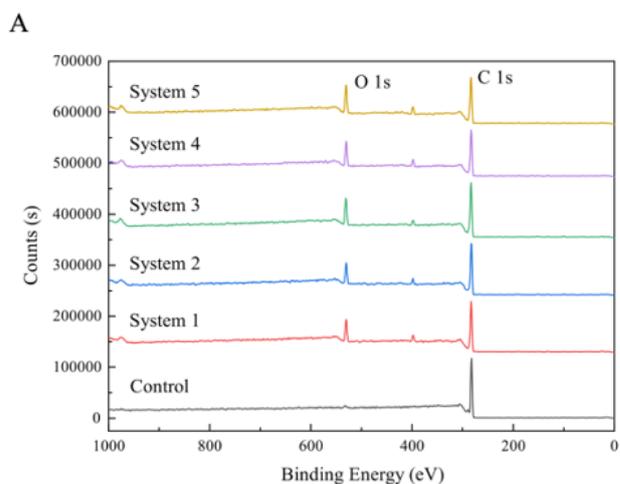
Figure 5. XPS scanning (A) and C1s spectra (B) of the control and PS after 60 h of biodegradation.

3.6. Variation of the molecular weight of PS

The molecular weight changes in PS before and after the enzymatic reaction were analyzed using GPC. The Mn values of the enzyme-treated PS were all lower than that of the control group, the Mw values of the enzyme-treated PS were all lower than that of the control group, except for reaction system 3.

A decrease in the molecular weight of a polymer is an important indicator of its degradation (Yang *et al.* 2018). This result shows that the long chains of PS molecules were depolymerized, and lower-molecular-weight degradation products were formed after 60 h of enzymatic reaction, which led to a decrease in molecular weight. Moreover, the reaction system with the largest reductions in the Mn and Mw values was system 5, indicating that system 5 had the strongest depolymerization of the long PS molecule chains. This result is in line with the results of FT-IR and XPS, where the number of hydroxyl groups on the surface of PS increases, the C-C bond decreases, and the formation of C-O bond means that part of the C-C bond in PS is oxidized to

alcohols and compounds similar to carboxylic acids, thereby reducing the molecular weight of PS.

Table 1. Changes in molecular weight of PS after 60 h of enzymatic degradation

Reaction system	Mn	Mn Reduction	Mw	Mw Reduction
Control	92,235	0.0	257,120	0.0
1	90,690	1.7	253,930	1.2
2	89,063	3.4	254,186	1.1
3	84,480	8.4	258,560	0.0
4	87,097	5.6	256,377	0.3
5	79,468	13.8	253,195	1.5

Mn, number-average molecular weight; Mw, heavy-average molecular weight.

3.7. 3.7 Thermogravimetric analysis of PS

The PS samples from the blank control group and five reaction systems were completely decomposed in the temperature range of 500–800°C under a nitrogen atmosphere. The PS weight loss curves for different reaction systems are shown in **Figure 6**. The temperatures of 5% PS weight loss were 407.01°C, 390.32°C, 401.08°C, 396.77°C, 398.21°C and 385.29°C for the blank control and reaction systems 1–5. The results show that the temperature of 5% PS weight loss in the blank control group was higher than that of 5% PS weight loss after the enzymatic reaction. This indicates that the thermal stability of PS decreased after enzymatic treatment, which could also indicate that the crystallinity, molecular weight, and polymer chain length of PS also decreased after enzymatic hydrolysis (Xiang *et al.* 2023; Sudhakar *et al.* 2008).
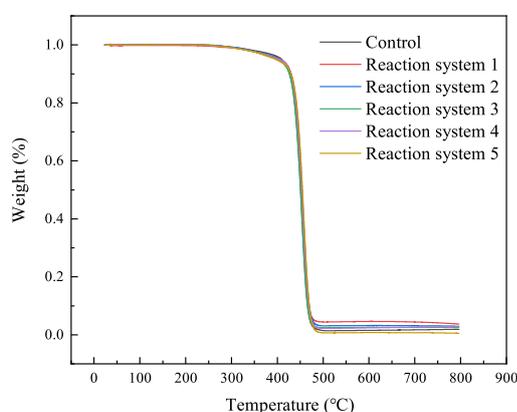
Figure 6. Thermogravimetric analysis of PS after 60 h of biodegradation.

4. Conclusions

Our study fills a gap in understanding of PS degradation by bioenzymes. Two oxidoreductases with potential PS-degrading abilities, AlkB and Adh, were isolated from *Acinetobacter. johnsonii* JUN01 and constructed in recombinant *E. coli*, which were successfully expressed, and the molecular weight is generally consistent with the expected protein molecular weight. The next step is to carry out enzyme activity tests and analyzed by SEM, WCA, FTIR, XPS, GPC, and TGA to determine the physicochemical properties of PS in the blank control group and after 60 h of enzymatic digestion. The results showed that AlkB and

Adh had the ability to degrade PS and proved that the synergistic degradation of PS by these two enzymes was feasible, indicating that we chose the target enzymes correctly. After enzymatic degradation, the C–C bond is broken to produce hydroxyl, carbonyl and C–O bonds. This result agrees with the conclusion of the theoretical analysis that has been reported previously, which supports the credibility of the results of this study (Kim *et al.* 2021).

As demonstrated by the characterization results, the changes in the physicochemical properties of PS in reaction system 5 (degradation of PS by AlkB-Adh composite enzyme) were always the most significant., These results indicate that the synergistic degradation of PS by these two enzymes is considerable provide a theoretical basis for the future investigation of the degradation efficiencies of both monoenzymatic and composite enzyme degradation using a quantitative analysis method.

In addition, since the reaction mechanism of PS with Adh is still unclear, the effect of coenzymes on the degradation reaction of the enzyme was also examined. The degradation activity of Adh existed under the action of both coenzymes, and that the composite enzymatic reaction of AlkB–Adh also existed under the action of both coenzymes. This provides support for future in-depth explanations of the Adh enzymatic reaction process.

Overall, study lays a solid foundation for the bioenzymatic degradation of PS and provides a feasible developmental direction. Future studies should also explore its enzymatic properties in depth or modify degradative enzymes using genetic engineering to improve their degradative enzymatic activity.

Availability of data and materials

All data used to supported the study are included within the manuscript.

Competing Interest

All of the authors declare there are no competing interests in publishing the manuscript.

References

Amobonye, A., Bhagwat, P.K., Singh, S. and Pillai, S. (2021). Plastic biodegradation: frontline microbes and their enzymes. *Science of The Total Environment* 759, 143536. https://doi.org/10.1016/j.scitotenv.2020.143536.

Anastasia Z. , Romanos S., George T., Maria K., Stamatina V., Georgios I. Z. and Evangelos T. (2023). Investigation of Abortiporus biennis lignocellulolytic toolbox, and the role of laccases in polystyrene degradation. *Chemosphere*. 312. https://doi.org/10.1016/j.chemosphere.2022.137338.

Arunrattiyakorn, P., Ponprateep, S., Kaennonsang, N., Charapok, Y., Punphuet, Y., Krajangsang, S., Tangteerawatana, P. and Limtrakul, A. (2022). Biodegradation of polystyrene by three bacterial strains isolated from the gut of Superworms (Zophobas atratus larvae). *Journal of Applied Microbiology* 132, 2823–2831. https://doi.org/10.1111/jam.15474.

Asmita, K., Shubhamsingh, T. and Tejashree, S. (2015). Isolation of plastic degrading micro-organisms from soil samples collected

at various locations in Mumbai, *Indian Journal Of Environmental Sciences* 4, 77–85.

Benson, N.U., Bassey, D.E. and Palanisami, T. (2021). COVID pollution: impact of COVID-19 pandemic on global plastic waste footprint. *Heliyon*. 7, e06343. https://doi.org/10.1016/j.heliyon.2021.e06343.

Chaudhary, A.K., Vijayakumar, R.P. (2020). Studies on biological degradation of polystyrene by pure fungal cultures. *Environment, Development and Sustainability* 22, 4495–4508. https://doi.org/10.1007/s10668-019-00394-5.

Chaurasia, M. (2020). Analytical review on biodegradation of plastic. *eLifePress*. 1, 1–8.

Cheng, Y., Chen, J.X., Bao, M.T. and Li, Y.M. (2022). Surface modification ability of Paracoccus sp. indicating its potential for polyethylene terephthalate degradation. *International Biodeterioration & Biodegradation* 173. https://doi.org/10.1016/j.ibiod.2022.105454.

Gabisa, E.W., Gheewala, S.H. (2022). Microplastics in ASEAN region countries: a review on current status and perspectives. *Marine Pollution Bulletin* 184, 114118. https://doi.org/10.1016/j.marpolbul.2022.114118.

Galgali, P., Varma, A.J., Puntambekar, U.S., Gokhale, D.V. (2002). Towards biodegradable polyolefins: strategy of anchoring minute quantities of monosaccharides and disaccharides onto functionalized polystyrene, and their effect on facilitating polymer biodegradation. *Chemical Communications*, 23, 2884–2885. https://doi.org/10.1039/b209254a.

Hou, L., Majumder, E.L.W. (2021). Potential for and distribution of enzymatic biodegradation of polystyrene by environmental microorganisms. *Materials (Basel)*. 14, 1–20. https://doi.org/10.3390/ma14030503.

Kiatkamjornwong, S., Sonsuk, M., Wittayapichet, S., Prasassarakich, P., Vejjanukroh, P.C. (1999). Degradation of styrene-g-cassava starch filled polystyrene plastics. Polymer Degradation and Stability 66, 323–335. https://doi.org/10.1016/S0141-3910(99)00082-8.

Kim, H.R., Lee, H.M., Yu, H.C., Jeon, E., Lee, S., Li, J., Kim, D.H. (2020). Biodegradation of Polystyrene by Pseudomonas sp. Isolated from the Gut of Superworms (Larvae of Zophobas atratus). *Environmental Science & Technology*, 54, 6987–6996. https://doi.org/10.1021/acs.est.0c01495.

Kim, H.R., Lee, H.M., Yu, H.C., Jeon, E., Lee, S., Li, J., Kim, D.H. (2020b). Biodegradation of polystyrene by pseudomonas sp. Isolated from the gut of superworms (larvae of Zophobas atratus). *Environmental Science & Technology*, 54, 6987–6996. https://doi.org/10.1021/acs.est.0c01495.

Kim, H.W., Jo, J.H., Kim, Y.B., Le, T.K., Cho, C.W., Yun, C.H., Chi, W.S., Yeom, S.J. (2021). Biodegradation of polystyrene by bacteria from the soil in common environments. *Journal of Hazardous Materials*, 416, 126239. https://doi.org/10.1016/j.jhazmat.2021.126239.

Kong, F., Hong, K.J., Xu, H., Zhao, S.G., Wang, Y.P. (2018). Evidence of polystyrene biodegradation by gut microbiota of Styrofoam-feeding yellow mealworms (larvae of Tenebrio molitor Linnaeus). *Microbiology China*, 45, 1438–1449. https://doi.org/10.13344/j.microbiol.china.170719.

Liu, H., Xu, J., Liang, R., Liu, J. (2014). Characterization of the medium- and long-chain n- alkanes degrading Pseudomonas aeruginosa strain SJTD-1 and its alkane hydroxylase genes. *PLOS ONE*. 9, e105506. https://doi.org/10.1371/journal.pone.0105506.

Mohan, A.J., Sekhar, V.C., Bhaskar, T., Nampoothiri, K.M., 206. (2016). Microbial assisted high impact polystyrene (HIPS) degradation. *Bioresource Technology* 213, 204–207. http://doi.org/10.1016/j.biortech.2016.03.021.

Mughal, A., Vikram, A., Ramarao, P. and Jena, G.B. (2010). Micronucleus and comet assay in the peripheral blood of juvenile rat: establishment of assay feasibility, time of sampling and the induction of DNA damage. *Mutation Research*, 700, 86–94. https://doi.org/10.1016/j.mrgentox.2010.05.014

Oikawa, E., Linn, K.T., Endo, T., Oikawa, T., Ishibashi, Y. (2003). Isolation and characterization of polystyrene degrading microorganisms for zero emission treatment of expanded polystyrene. *Environmental Engineering Research* 40, 373–379.

Orona-Návar, C., García-Morales, R., Loge, F.J., Mahlknecht, J., Aguilar-Hernández, I. and Ornelas-Soto, N. (2022). Microplastics in Latin America and the Caribbean: a review on current status and perspectives. *Journal of Environmental Management* 309, 114698. https://doi.org/10.1016/j.jenvman.2022.114698.

Peng, R.T., Xia, M.L., Ru, J.K., Huo, Y.X. and Yang, Y. (2018). Microbial degradation of polyurethane plastics. *Sheng Wu Gong Cheng Xue Bao.* 34, 1398–1409. https://doi.org/10.13345/j.cjb.170532.

Shang, J., Chai, M., Zhu, Y. (2003). Solid-phase photocatalytic degradation of polystyrene plastic with TiO2 as photocatalyst. *Journal of Solid State Chemistry* 174, 104–110. https://doi.org/10.1016/S0022-4596(03)00183-X.

Subramani, M., Sepperumal, U. (2017). GCMS analysis of pseudomonas sp., mediated degradation of polystyrene. *Annals of Biological Research* 8, 8–11.

Sudhakar, M., Doble, M., Murthy, P.S., Venkatesan, R. (2008). Marine microbe-mediated biodegradation of low- and high-density polyethylenes. *International Biodeterioration & Biodegradation* 61, 203–213. https://doi.org/10.1016/j.ibiod.2007.07.011.

Urbanek, A.K., Rybak, J., Wróbel, M., Leluk, K., Mirończuk, A.M. (2020). A comprehensive assessment of microbiome diversity in Tenebrio molitor fed with polystyrene waste. Environmental Pollution 262, 114281. https://doi.org/10.1016/j.envpol.2020.114281.

Verla, A.W., Enyoh, C.E., Verla, E.N., Nwarnorh, K.O. (2019). Microplastic–toxic chemical interaction: a review study on quantified levels, mechanism and implication. *SN Applied Sciences* 1, 1400. https://doi.org/10.1007/s42452-019-1352-0.

Xiang, P., Zhang, Y., Zhang, T., Wu, Q., Zhao, C., Li, Q. (2023). A novel bacterial combination for efficient degradation of polystyrene microplastics. *Journal of Hazardous Materials* 458, 131856. https://doi.org/10.1016/j.jhazmat.2023.131856

Yang, L., Liu, Y., Gao, J., Peng, X.W., Bai, Z.H., Zhuang, X.L. (2020). Biodegradation of expanded polystyrene foams in Zophobas morio: effects of gut microbiota. *Huan Jing Ke Xue.* 41, 5609–5616. https://doi.org/10.13227/j. hjkx. 202003273.

Yang, S.S., Brandon, A.M., Andrew Flanagan, J.C.A., Yang, J., Ning, D., Cai, S.Y., Fan, H.Q., Wang, Z.Y., Ren, J., Benbow, E., Ren, N.Q., Waymouth, R.M., Zhou, J., Criddle, C.S., Wu, W.M. (2018). Biodegradation of polystyrene wastes in yellow mealworms (larvae of Tenebrio molitor Linnaeus): factors affecting biodegradation rates and the ability of polystyrene-

fed larvae to complete their life cycle. *Chemosphere*. 191, 979–989. https://doi.org/10.1016/j.chemosphere.2017.10.117.

Yoshida, S., Hiraga, K., Takehana, T., Taniguchi, I., Yamaji, H., Maeda, Y., Toyohara, K., Miyamoto, K., Kimura, Y., Oda, K. (2016). A bacterium that degrades and assimilates poly(ethylene terephthalate). *Science*. 351, 1196–1199. https://doi.org/10.1126/science.aad6359.

Zhang, T., Liu, P., Wang, Q., Liang, Q. and Qi, Q. (2021). Degradation of petroleum- based plastics bymicrobes and microbial consortia. *Sheng Wu Gong Cheng Xue Bao* 37, 3520–3534. https://doi.org/10.13345/j.cjb.210399.